Investigation of Texture Quantification Parameters for Neurological PET Image Analysis

Ivan S. Klyuzhin*, Stephan Blinder*, Rostom Mabrouk*, Arman Rahmim†, Vesna Sossi*
* Department of Physics and Astronomy, University of British Columbia, Vancouver, BC, V6T1Z1; Email: ivansk@physics.ubc.ca
† Department of Radiology, Johns Hopkins University, Baltimore, MD 21287

***Abstract*—We investigate the correlation between the clinical severity of neurodegenerative disease and texture metrics (such as Haralick features) computed using PET images of the brain. Specifically, we explore how the parameters of feature computation - such as the region of interest definition method, and the direction and distance used for texture quantification - affect the correlation between texture-based image metrics and clinical disease severity. The analysis was based on an ongoing Parkinson's disease imaging study, with co-registered PET and MRI images, and tracer predominantly concentrated in the striatum. Disease duration was used as the primary clinical metric. It was found that the region of interest placement method substantially affected the correlation values. Significant correlation ($p<0.01$) was obtained when simple box-like regions were used instead of the anatomic MRI-based regions. The used direction affected the correlation values moderately, and distance did not have a pronounced effect. The results suggest that the Haralick features and other texture metrics that do not require kinetic modeling could be potentially used for the analysis of PET images for which the corresponding MRI data are not available. The results also show that the region of interest definition method and the direction along which metrics are computed may affect metric performance.**

I. Introduction

Clinical and pre-clinical studies of neurological disorders often utilize positron emission tomography (PET) imaging to obtain information about the physiological processes in-vivo. Traditional analysis of the PET tracer distribution in the brain is based either on computing the standard uptake values (SUV), or using tracer kinetic modeling (KM) to obtain parameters such as non-displaceable binding potential (BP_{ND}). However, the computation of BP_{ND} may be difficult as it requires dynamic scanning and knowledge of the tracer input function. Therefore, it is of interest to develop new PET image quantification methods and metrics that are based on simpler scanning procedures and that provide additional information relevant to the disease.

We have previously shown that in Parkinson's disease (PD) subjects, texture and shape metrics evaluated on the images of [11C]-dihydrotetrabenazine (DTBZ, marker of the vesicular monoamine transporter type 2) tracer distribution in striatum have significant correlation with disease severity and duration [1], [2]. Other texture-based metrics, such as the Haralick features (HF) computed from the gray level co-occurrence matrix (GLCM), have also been found to correlate with the clinical PD severity assessments [3], [4], and contribute to automatic detection of disease [5]. These metrics do not require KM.

The literature on application of HF in the analysis of emission images has been primarily focused on oncology [6], [7] and proper translation of these features to neurological analysis requires careful attention. For instance, in oncology the GLCM is typically computed along 2 or 3 orthogonal directions and averaged [8], [9]. This method is consistent with the fact that tumor growth typically does not have a preferred direction, or such direction is unknown apriori. On the other hand, in PD a clear directionality (gradient) in the tracer uptake is present due to the specific (and known) pattern of the dopaminergic function loss (Fig. 1) [10].

In this work, we evaluate how the texture quantification parameters affect the correlation between the texture-based image metrics and clinical disease duration. The study was performed using co-registered high-resolution PET and MRI images of PD subjects, with tracer (DTBZ) predominantly concentrated in the striatum, a dopamine-rich area. The following parameters were explored: 1) GLCM direction, 2) GLCM distance, 3) the method of region-of-interest (ROI) definition. Based on the previous results, the chosen image metrics for this analysis consisted of HF, J1 and J2 moment invariants (MI), and the mean BP_{ND} in the ROI.

II. Methods

A. Clinical and image data

The analysis was performed using DTBZ activity concentration images and parametric BP_{ND} images for 37 PD subjects. Disease duration from the time of clinical onset was used as a clinical measure of disease. The mean disease duration was 5.7±4.2 years (range 0 to 13 years). The PET data were acquired in list-mode using the Siemens High Resolution Research Tomograph (HRRT). The images were reconstructed using OSEM-OP (256×256×207, voxel size 1.22 mm). The DTBZ activity concentration images were reconstructed from coincidence data acquired in the time period 30-60 minutes post-injection. Parametric DTBZ BP_{ND} images were produced from 16 temporal frames using a simplified reference tissue model [11]. PET images were rigidly co-registered to MR images of the subjects. The MR images (256×256×170, voxel size 1.0 mm) were obtained with a Philips Achieva 3T scanner using a T1-weighted Turbo Field Echo sequence. The

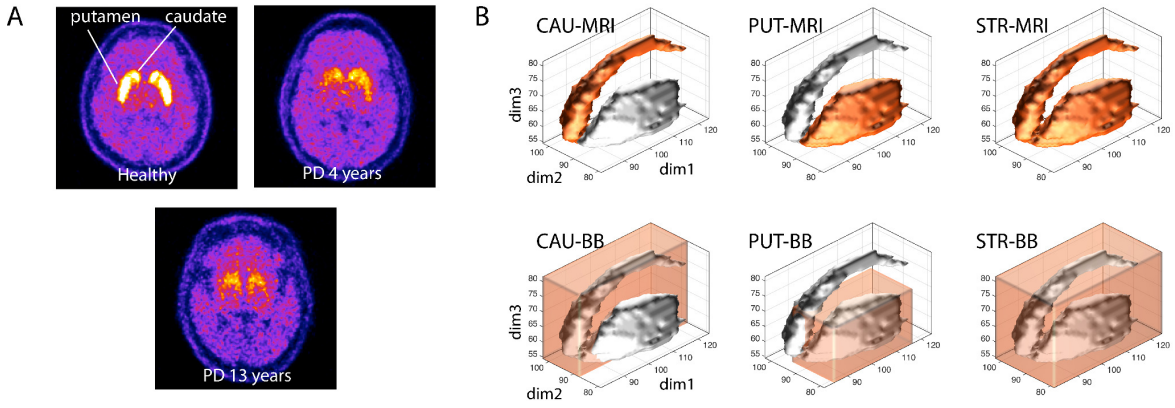

Fig. 1. A - DTBZ images of a healthy subject and two PD subjects. B - examples of the MRI-based ROIs of the caudate (CAU-MRI), putamen (PUT-MRI), and striatum (STR-MRI), and the corresponding bounding box ROIs (CAU-BB, PUT-BB, STR-BB).

SPM package (www.fil.ion.ucl.ac.uk/spm) was used for the mutual information-based PET-MRI image registration.

B. Image metrics

The analyzed image metrics included GLCM-based Haralick features, J1 and J2 moment invariants, and the mean value of DTBZ BP_{ND} within the ROI. The Haralick features represent a group of measures extracted from GLCM, which counts the co-occurring gray levels between pairs of voxels, located at the end points of the stepping vector $\mathbf{g} = D \times \hat{\mathbf{g}}$. At least three parameters must be defined to compute GLCM of a given image: a) the number of gray-level bins used for the voxel-value discretization, b) direction $\hat{\mathbf{g}} = (x, y, z)$ along which the gray-value co-occurrences are counted, and c) distance D between the analyzed voxel pairs (distance along the normalized direction vector $\hat{\mathbf{g}}$). Although many different HF can be computed from a single GLCM (mathematical definitions can be found in [12], [13]), for this study we have chosen a subset of HF that have shown statistically significant correlation with disease duration in a preliminary analysis: autocorrelation (AUTOC), correlation (CORR), cluster shade (CLSHADE), energy (ENER), information measure 1 (INF1) and 2 (INF2), maximum probability (MAXPR), sum average (SUMAVG), and sum entropy (SUMENT).

The moment invariants J1 and J2 have shown high correlation with disease duration in previous work [1], [2]. Although the exact meaning of the moment invariants may be difficult to interpret, the J1 can be understood as a measure of distance-weighted variance of activity values within the analyzed region, and the J2 moment is a measure of covariance.

Note that HF and MI metrics were computed directly from the 30-minute DTBZ activity concentration images. In contrast, the mean DTBZ BP_{ND} in the ROI was computed from the parametric binding potential images. Since BP_{ND} is often used as the primary metric in neuroimaging studies, we used it as a reference.

C. Explored texture quantification parameters

In this work, we investigated the effect of the following parameters on the correlation between image metrics and disease duration:

1) GLCM direction $\hat{\mathbf{g}}$ (only influences HF metrics). The analyzed GLCM directions included: a) Anatomic direction - along the longitudional anatomical axis of the analyzed brain structure; this direction was determined as the first principal component resulting from the PCA analysis on the data (x, y, z), where x, y, z are the coordinates of voxels comprising the MRI ROI; b) PET direction - the average direction of PET activity gradient in the ROI; c) directions of image dimensions - posterior-anterior (dim1), left-right(dim2) and inferor-superior (dim3); d) average direction GLCM - in this case three GLCMs were computed along dim1, dim2 and dim3 and then averaged; the HF metric values were computed using the averaged GLCM. PUT-MRI ROIs were used investigate different GLCM directions.

2) GLCM distance D (only influences HF metrics). We investigated GLCM distances equal to 1, 2, 3, 4 and 5 voxels using PUT-MRI ROIs.

3) ROI definition method (influences all metrics). We tried using two types of ROIs for three brain structures of interest (putamen, caudate, and striatum which included putamen and caudate) (Fig. 1). The MRI-based anatomical ROIs (PUT-MRI, CAU-MRI, STR-MRI) were obtained by manually outlining the corresponding brain structure in the MRI images.

The bounding box ROIs (PUT-BB, CAU-BB, STR-BB) were defined around the corresponding MRI ROIs with sides parallel to the image dimensions, and were equal in size to the extent of the MRI ROIs along those dimensions (dim1, dim2, dim3). The bounding box ROIs represent a simplified method of ROI placement and definition, which can be used when anatomic images are not available. For the ROI investigation we used $D_{glcm} = 3$ voxels to compute the GLCM (neighboring voxels are known to be correlated in PET images, and large distances reduce the total number of GLCM counts).

TABLE I
SPEARMAN'S CORREALTION COEFFICIENT ρ MEASURED FOR DIFFERENT GLCM DIRECTIONS (PUT-MRI ROI)

	AUTOC	CORR	CLSHADE	ENER	INF1	INF2	MAXPR	SUMAVG	SUMENT
[1 0 0]	-0.64**	-0.09	0.46**	0.57**	0.13	-0.14	0.49**	-0.58**	-0.46**
[0 1 0]	-0.58**	-0.01	0.54**	0.40*	0.02	-0.02	0.57**	-0.57**	-0.18
[0 0 1]	-0.64**	-0.04	0.49**	0.58**	0.05	-0.09	0.56**	-0.59**	-0.42**
PET	-0.55**	0.02	0.52**	0.46**	-0.01	0.00	0.60**	-0.52**	-0.13
MRI	-0.65**	-0.11	0.47**	0.51**	0.14	-0.18	0.50**	-0.62**	-0.44**
AVER	-0.63**	0.00	0.52**	0.57**	0.01	-0.03	0.58**	-0.60**	-0.37*

$^{*}p < 0.05$ $^{**}p < 0.01$

TABLE II
SPEARMAN'S CORREALTION COEFFICIENT ρ MEASURED FOR DIFFERENT BRAIN STRUCTURES AND ROI TYPES

	AUTOC	CORR	CLSHADE	ENER	INF1	INF2	MAXPR	SUMAVG	SUMENT	J1	J2	BP_{ND}
CAU-MRI	-0.17*	-0.01	0.29	0.31	-0.04	0.01	0.15	-0.17	-0.27	0.50**	0.54**	-0.65**
CAU-BB	0.40*	-0.25	-0.53**	-0.54**	0.22	-0.11	-0.36*	0.40*	0.40*	0.40*	0.38*	-0.54**
PUT-MRI	-0.64**	-0.09	0.46**	0.57**	0.13	-0.14	0.49**	-0.58**	-0.46**	0.61**	0.62**	-0.80**
PUT-BB	0.17	-0.54**	-0.46**	-0.12	0.55**	-0.59**	-0.28	0.32	-0.53**	0.47**	0.47**	-0.71**
STR-MRI	-0.36*	0.07	0.47**	0.39*	-0.01	0.00	0.44**	-0.37*	-0.22	0.57**	0.57**	-0.78**
STR-BB	0.42**	-0.46**	-0.62**	-0.46**	0.33*	-0.24	-0.49**	0.48**	0.11	0.44**	0.41*	-0.62**

$^{*}p < 0.05$ $^{**}p < 0.01$

With PUT-MRI and PUT-BB ROIs the GLCM was computed for direction $\hat{\mathbf{g}} = dim1$; otherwise, average-direction GLCM was computed.

We used 16 gray levels to quantize activity voxel values. GLCMs were normalized by the total number of counts. All image metrics were computed within the ROIs defined on the less affected by the disease side of the brain. The Spearman's correlation coefficient ρ was used as the measure of correlation between the image metrics and disease duration.

III. RESULTS

A. Effect of GLCM direction on correlation

The values of ρ corresponding to different GLCM directions in putamen are given in Table I. The differences in ρ between different directions were relatively small; the ENER and SUMENT metrics may be considered exception where the difference in ρ was more substantial and different directions produced different p-values. PET and dim2 directions produced very similar ρ values, as well as directions MRI and dim1. Using the average direction GLCM produced similar ρ values to GLCMs computed along specific directions. In the caudate, the values of ρ were unaffected by the GLCM direction.

The differences in GLCM values computed using different directions were relatively minor. Generally, GLCMs computed using the MRI and dim1 directions had higher number of counts in the low gray level quarter (values 1-4); with other directions, the counts were spread more uniformly along the main diagonal.

B. Effect of GLCM distance on correlation

Distance D had a strongly pronounced effect on the spatial distribution of counts in the GLCM. Using low D (1, 2 voxels) resulted in GLCMs with the majority of counts falling along the main diagonal. On the other hand, with high D (4, 5 voxels) the counts were more evenly distributed across the non-diagonal elements. Using grater D also resulted in lower total number of the co-occurrence counts (as expected given the finite size of the ROIs): 7000 counts with $D = 1$, 4000 with $D = 5$.

Although the effect of D on the count distribution in GLCM was very pronounced, the correlation coefficients were less affected, and the dependence of ρ on D did not have a consistent pattern for all HF metrics. The values of ρ for AUTOC and CLSHADE did not depend on D. On the other hand, the correlation values for the ENER and ENTRO metrics were affected: the correlation tended to increase with greater distance, and the difference in ρ between $D_{glcm} = 1$ and $D_{glcm} = 5$ was on the order of 0.1-0.3 points. It should be noted that in the cases where distance did influence the correlation, the ρ values were relatively low (range between 0.1 and 0.5).

C. Effect of ROI definition on correlation

Among the investigated parameters, the ROI definition method had the greatest impact on the correlation (Table II). In caudate, the correlation for most metrics was generally weak using both CAU-MRI and CAU-BB ROIs. For several metrics (e.g. CLSHADE and ENER), the values of ρ were notably higher with CAU-BB ROIs, with accompanying differences in the significance levels. The same pattern was also observed in putamen: using the bounding box ROIs as opposed to the MRI ROIs resulted in higher ρ for CORR, INF1, INF2, and SUMENT and lower ρ for AUTOC, ENER, MAXPR, and SUMAVG. The value of ρ for CLSHADE had different signs

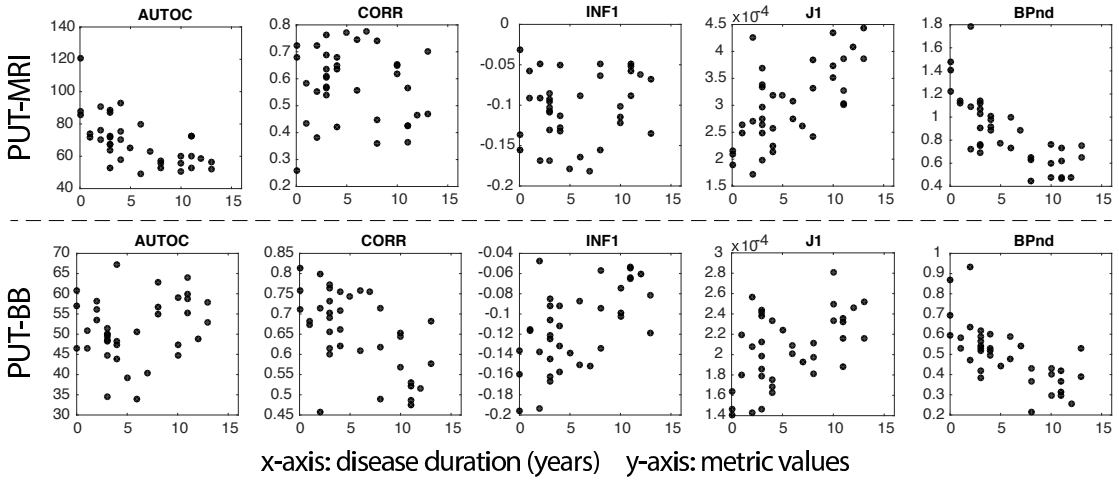

Fig. 2. Comparison of the scatter plots (metric value vs. disease duration) between MRI-based (PUT-MRI) and bounding box ROI (PUT-BB) of the putamen.

with PUT-MRI and PUT-BB ROIs. The ρ values for J1, J2 and BP_{ND} were lower with bounding box ROIs. Overall, BP_{ND} had the strongest correlation with disease duration regardless of the used ROI.

Scatter plots of the metric values versus disease duration are shown in Figure 2 for the PUT-MRI and PUT-BB ROIs. The plots demonstrate that the high measured correlation coefficients were not biased by a small number of outliers. The difference in correlation between the MRI-defined and bounding box ROIs is clearly visible in from the graphs. For example, data points in the INF1 and CORR plots better fit to a line with PUT-BB ROI (the opposite effect can be seen with AUTOC, J1 and BP_{ND}).

IV. Conclusions

We found statistically significant correlations between several investigated texture metrics and PD duration. While MI have been previously shown to have a very strong correlation with PD duration and clinical severity, in this work we also demonstrate that the previously unexplored information metrics INF1 and INF2, as well as several other HF metrics, have relatively strong and significant ($p < 0.01$) correlation with disease duration.

While J1, J2 and BP_{ND} had significant correlation with disease duration in all considered brain structures (putamen, caudate or striatum) and with both tested ROI definition methods (MRI-defined or bounding box), the correlation values obtained with HF metrics were structure- and ROI-dependent. Therefore, in the analysis of tracer distribution pattern using texture-based approaches, the analysis outcome may strongly depend on the appropriate feature selection method.

Our results demonstrate that the chosen GLCM direction and distance may influence the measured correlation values. In this study, there was no single preferred direction that maximized the correlation values for all metrics, but nonetheless the correlation values for some HF metrics varied between different directions. Using the average direction GLCM produced correlation values similar to those obtained when single direction was chosen. Based on this result, we conclude that in the analysis of brain imaging with disease-specific spatio-temporal patterns, using the average-direction GLCM would not result in substantial degradation of the measured statistical correlations.

The method of ROI definition had a strong impact on which image metrics were correlated with disease duration. With bounding box ROIs, HF metrics such as INF1 and INF2 were found to have significant correlation with disease duration. This observation points to the fact that the MRI-based ROIs may not be necessary for texture-based analysis, and an approximately-placed ROIs may be used instead. In addition, the correlation values for J1, J2 and BP_{ND} were also relatively well preserved when bounding box ROIs were used compared to the MRI-based ROIs.

References

[1] I. S. Klyuzhin, M. Gonzalez, E. Shahinfard, N. Vafai, and V. Sossi, "Exploring the use of shape and texture descriptors of positron emission tomography tracer distribution in imaging studies of neurodegenerative disease," *Journal of Cerebral Blood Flow & Metabolism*, Oct. 2015.

[2] M. E. Gonzalez, K. Dinelle, N. Vafai, N. Heffernan, J. McKenzie, S. Appel-Cresswell, M. J. McKeown, a. J. Stoessl, and V. Sossi, "Novel spatial analysis method for PET images using 3D moment invariants: Applications to Parkinson's disease." *Neuroimage*, vol. 68, pp. 11–21, Mar. 2013.

[3] A. Rahmim, J. Coughlin, M. Gonzalez, C. J. Endres, Y. Zhou, D. F. Wong, R. L. Wahl, V. Sossi, and M. G. Pomper, "Novel parametric PET image quantification using texture and shape analysis," in *2012 IEEE Nuclear Science Symposium and Medical Imaging Conference Record (NSS/MIC)*. IEEE, Oct. 2012, pp. 2227–2230.

[4] S. Blinder, I. Klyuzhin, M. Gonzalez, A. Rahmim, and V. Sossi, "Texture and Shape Analysis on High and Low Spatial Resolution Emission Images," in *2014 IEEE Nuclear Science Symposium and Medical Imaging Conference Record (NSS/MIC)*. Seattle, WA: IEEE, 2014.

[5] F. J. Martinez-Murcia, J. M. Gorriz, J. Ramirez, M. Moreno-Caballero, and M. Gomez-Rio, "Parametrization of textural patterns in 123I-ioflupane imaging for the automatic detection of Parkinsonism," *Medical Physics*, vol. 41, no. 1, p. 012502, 2014.

[6] M. Hatt, M. Majdoub, M. Vallières, F. Tixier, C. C. Le Rest, D. Groheux, E. Hindié, A. Martineau, O. Pradier, R. Hustinx, R. Perdrisot, R. Guillevin, I. El Naqa, and D. Visvikis, "18F-FDG PET uptake characterization through texture analysis: investigating the complementary nature of heterogeneity and functional tumor volume in a multi-cancer site patient cohort." *Journal of nuclear medicine : official publication, Society of Nuclear Medicine*, vol. 56, no. 1, pp. 38–44, Jan. 2015.

[7] J. Yan, J. L. Chu-Shern, H. Y. Loi, L. K. Khor, A. K. Sinha, S. T. Quek, I. W. K. Tham, and D. Townsend, "Impact of Image Reconstruction Settings on Texture Features in 18F-FDG PET." *Journal of nuclear medicine : official publication, Society of Nuclear Medicine*, vol. 56, no. 11, pp. 1667–73, Nov. 2015.

[8] I. El Naqa, P. Grigsby, A. Apte, E. Kidd, E. Donnelly, D. Khullar, S. Chaudhari, D. Yang, M. Schmitt, R. Laforest, W. Thorstad, and J. O. Deasy, "Exploring feature-based approaches in PET images for predicting cancer treatment outcomes." *Pattern recognition*, vol. 42, no. 6, pp. 1162–1171, Jun. 2009.

[9] F. Orlhac, M. Soussan, J.-A. Maisonobe, C. a. Garcia, B. Vanderlinden, and I. Buvat, "Tumor texture analysis in 18F-FDG PET: relationships between texture parameters, histogram indices, standardized uptake values, metabolic volumes, and total lesion glycolysis." *Journal of nuclear medicine : official publication, Society of Nuclear Medicine*, vol. 55, no. 3, pp. 414–22, Mar. 2014.

[10] A. B. Newberg and A. Alavi, "Normal Patterns and Variants in PET Brain Imaging," *PET Clinics*, vol. 5, no. 1, pp. 1–13, Jan. 2010.

[11] R. N. Gunn, A. A. Lammertsma, S. P. Hume, and V. J. Cunningham, "Parametric imaging of ligand-receptor binding in PET using a simplified reference region model." *NeuroImage*, vol. 6, no. 4, pp. 279–87, Dec. 1997.

[12] R. M. Haralick, K. Shanmugam, and I. Dinstein, "Textural Features for Image Classification," *IEEE Transactions on Systems, Man, and Cybernetics*, vol. 3, no. 6, pp. 610–621, Nov. 1973.

[13] L.-K. Soh and C. Tsatsoulis, "Texture analysis of SAR sea ice imagery using gray level co-occurrence matrices," *IEEE Transactions on Geoscience and Remote Sensing*, vol. 37, no. 2, pp. 780–795, Mar. 1999.